Research Article J. Electrochem. Sci. Technol., 2018, 9(4), 330-338

Journal of Electrochemical Science and Technology
jecst.org

Structural Effect of Conductive Carbons on the Adhesion and Electrochemical Behavior of $LiNi_{0.4}Mn_{0.4}Co_{0.2}O_2$ Cathode for Lithium Ion Batteries

Mohammed Latifatu[1], Chris Yeajoon Bon[1], Kwang Se Lee[1], Louis Hamenu[2], Yong Il Kim[3], Yun Jung Lee[3], Yong Min Lee[4], and Jang Myoun Ko[1]*

[1]*Department of Applied Chemistry & Biotechnology, Hanbat National University, 125 Dongseo-daero, Yuseong-gu, Daejeon 34152, Republic of Korea*

[2]*Department of Chemistry School of Physical and Mathematical Sciences, College of Basic and Applied Sciences, University of Ghana, Legon, Ghana*

[3]*Department of Energy Engineering, Hanyang University, 222 Wangsimni-ro, Seongdong-gu, Seoul 04763, Republic of Korea*

[4]*Department of Energy Science and Engineering, Daegu Gyeongbuk Institute of Science & Technology, 333 Techno Jungang-daero, Hyeonpung-myeon, Dalseong-gun, Daegu 42988, Republic of Korea*

ABSTRACT

The adhesion strength as well as the electrochemical properties of $LiNi_{0.4}Mn_{0.4}Co_{0.2}O_2$ electrodes containing various conductive carbons (CC) such as fiber-like carbon, vapor-grown carbon fiber, carbon nanotubes, particle-like carbon, Super P, and Ketjen black is compared. The morphological properties is investigated using scanning electron microscope to reveal the interaction between the different CC and the active material. The surface and interfacial cutting analysis system is also used to measure the adhesion strength between the aluminum current collector and the composite film, and the adhesion strength between the active material and the CC of the electrodes. The results obtained from the measured adhesion strength points to the fact that the structure and the particle size of CC additives have tremendous influence on the binding property of the composite electrodes, and this in turn affects the electrochemical property of the configured electrodes.

Keywords : Conductive carbons, Composite electrodes, Adhesion property, Lithium ion batteries, Surface and interfacial cutting analysis system

Received : 8 June 2018, Accepted : 8 August 2018

1. Introduction

The cycling performance of the cathode and the anode is seriously affected by the adhesion between the active material and the current collectors [1,2]. The polymeric binder plays the role of holding the electrode film (active material and conducting agent) to the current collector. Electrodes in commercial lithium ion batteries (LIB) contain about 2-5% binder, which is very small compared to the total mass of the electrode. Nonetheless, without this binder the contact between the current collector and the active material is compromised. Experimental investigations have been dedicated to finding a suitable binder for LIB [3-6]. Lui et al. investigated the polymeric binder and particle interaction as a factor in determining electrode performance [7]. The conductive additive is another small but important component of the LIB electrode. It occupies about 3-5% of the total mass of the electrode. Graphite, metal powder, metal fibers, and carbon nanomaterials have been considered as conductive additives [8-10]. Among these particles,

*E-mail address: jmko@hanbat.ac.kr

DOI: https://doi.org/10.5229/JECST.2018.9.4.330

carbon nanomaterials have been widely used in LIB electrodes due to their excellent electrical and thermal conductivity [11-13], high aspect ratio [14], and ease of preparation. Two types of conductive carbons (CC) can be defined based on their morphological structure: fiber-like CC such as carbon nanotubes (CNT), vapor-grown carbon fiber (VGCF), and metal fibers, and particle-like CC such as Super P (SP), Ketjenblack (KB), and graphite. The different morphological structures found in various CC produce different conducting properties as well as unique interactions between the active material and the binder. The mechanical integrity of the electrode material is measured by the contact between the current collector and the composite film (active material/conducting additive/binder). In addition, the particle size, structure, and aspect ratio of the active material and the conductive material greatly impact the adhesion strength and the electrochemical performance of the electrode [15,16]. Besides conducting electrons between the particles of the composite film, CC also forms an electronic conductive channel between the current collector surface and the composite film [17-19]. Tensile pull test [20], 180° peeling test [21] and push-out bond strength technique [22] have been developed and employed in measuring the adhesion property of coated materials. Recently, some researchers have utilized surface and interfacial cutting analysis system (SAICAS) to measure the actual adhesion strength of the composite film to the current collector at a specific depth. They have investigate and discussed intensively the operation and utilization of SAICAS in electrode characterization [22-25].

We studied the effect of fiber-like and particle-like CC on the adhesion and electrochemical performance of lithium nickel manganese cobalt oxide (NMC). The different physical and chemical properties of the materials making up the cathode may trigger different interactions between the various components. In order to develop longer-lasting LIBs, these physical and chemical interactions must be understood and controlled. SAICAS was used to measure the adhesion strength between the composite film and the current collector, and the adhesion strength between the particles of the composite film. In addition, the electrochemical performance was probed using cyclic voltammetry and charge-discharge.

Table 1. Physical properties of the different conductive carbons.

	Diameter (nm)	Lenth (um)	BET Surface area (m^2/g)	Particle size (nm)
CNT	55	10.-30	60	-
VGCF	150	10-20	13	-
KB	-	-	7850	30
SP	-	-	62	40

2. Experimental

2.1 Cathode fabrication

NMC cathode was prepared by casting a slurry consisting of 93% (NMC, Ecopro, Korea) as active material, 4 wt.% of SP (TIMCAL SUPER P^{TM}), VGCF (Showa Denko), KB (EC 300 J, AkzoNobel), or CNT (LG Chem, South Korea) as conductive additive, and 3 wt.% polyvinylidene fluoride (PVdF, Kreha, Japan, $M_w \approx 350{,}000$) as polymeric binder in *N*-methyl-2-pyrrolidone (NMP, Sigma Aldrich). The physical properties of the different CC are depicted in Table 1. The viscous slurry was cast on an aluminum foil (15 μm, San-A Aluminum, Korea) via doctor blade apparatus. The coated slurry was dried at 120°C for 2 h and then pressed with a roll pressing machine (WV-60, Samyang 60, South Korea). A composite electrode without conductive carbon was also prepared for comparison. The thickness, densities, and loading levels were controlled to about 49 μm, 2.1 g cm^{-3} and 15 mg cm^{-2} respectively, for all the composite electrodes.

2.2 Electrode characterization

The surface morphology and electrical resistance of the electrodes were measured using field-emission scanning electron microscope (FE-SEM, HITACHI SU5000, Japan) and linear four-probe system (CMT-100, AIT-TU, Korea). For the surface resistance measurement, the dried and pressed electrodes, consisting of the cathode material, the CC and the PVDF binder was used. The cathodes were cut using an argon-ion milling system (Hitachi IM4000Plus, Japan) for cross-sectional analysis. The adhesion strength between the particles of the composite film (A_{mid}), and the composite film and the current collector ($A_{C/Al}$) were measured using SAICAS (Diapla Winters Company limited, Japan). A boron nitride blade with a

width of 1 mm, fixed at a shear angle of 45° was used. To measure the adhesion strength between the composite and the current collector ($A_{C/Al}$), the blade of the instrument moves vertically with a fixed load of 0.5 N until it contacts the current collector where the vertical force is changed to 0.2 N (region A, Fig. 3a). The blade then moves in the horizontal direction employing this new vertical force (region B, Fig. 3a). The results were measured at a constant vertical fixed load mode. On the other hand, the adhesion strength between the particles of the composite (A_{mid}) was measured at a constant rate mode. In a typical A_{mid} measurement, the blade moves with a speed of 0.2 $\mu \cdot ms^{-1}$ in the vertical direction until it gets to the center of the coated film (region A, Fig. 3b) and then move in the horizontal direction (region B, Fig. 3b). $A_{C/Al}$ and A_{mid} were obtained by dividing the horizontal forces in each case by the width of the blade.

2.3 Full cell preparation

The electrodes were punched into a spherical disc with a diameter of 14 mm. The half cells assembled in a coin-type cell (2032) and in an argon-filled glove box consisting of lithium metal (16 mm, 99.99% Aldrich) as counter and reference electrode, and NMC with the different CC as the working electrode. 1.2 M $LiPF_6$ (EC/DMC =1:3 volume ratio) and polyethylene separator (PE, 18 mm, 20 μm, celgard) were used as the electrolyte and separator, respectively.

2.4 Electrochemical characterization

Cyclic voltammograms (CVs) of the cathode with the different CC were measured at a scan rate of 0.1 mV s^{-1} and a potential range of 2.5-4.4 V using Autolab (ECO CHEMIE PGSTAT 100). Charge and discharge tests were measured at room temperature in the potential range of 2.8-4.4 V, charging in constant current/constant voltage (CC/CV) mode at 0.1 C-rate and discharging at 0.1, 0.2, 0.5, 1, 2, and 5 C in CC mode using a battery cycler (PNE Solution, Korea). The cycle performance was measured for 100 cycles, charging in CC/CV mode at 1 C and discharging at 1 C in CC mode at the same voltage range. The rate performance was conducted at increasing rates of 0.2, 0.5, 1, 2, and 5 C for charging (CC/CV mode) and discharging (CC mode) in the voltage range of 2.8-4.4 V. All the cells were kept for 6 h before electrochemical measurement.

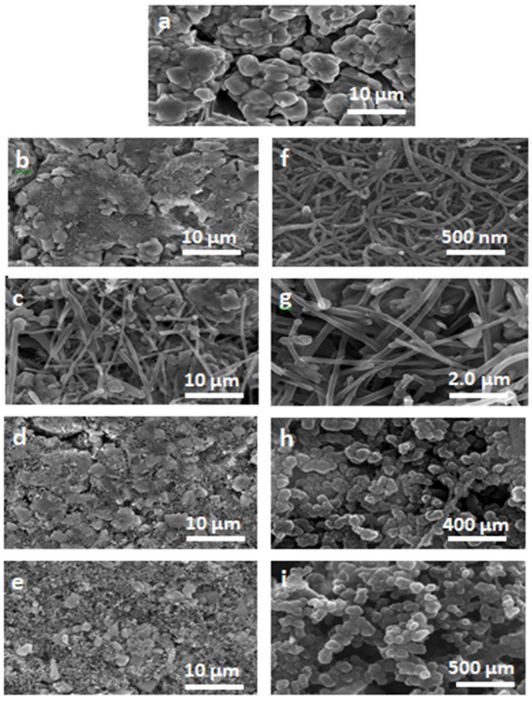

Fig. 1. FESEM images of the surfaces of the composites (a) NMC, (b) NMC-CNT, (c) NMC-VGCF, (d) NMC-KB, and (e) NMC-SP, and the conductive carbons (f) CNT, (g) VGCF, (h) KB, and (i) SP.

3. Results and Discussion

SEM images show the surface morphology of the composite electrodes and the different CC in Fig.1. From Fig. 1a, the pure NMC electrode exhibited aggregates of primary particles (average particle size around 50 nm) into secondary particles with an average particle size of 10 μm. The composite with KB and SP showed spherical particles (see Fig. 1h and 1i), which easily fill the spaces between the secondary particles of the NMC (see Fig. 1d and 1e). These particle-like CC were also uniformly dispersed on the surfaces of the secondary particles of NMC. On the other hand, the fiber-like CC (CNT and VGCF) showed a wire-type morphology (see Fig. 1f and 1g) connecting the particles of the active material. Looking at the composites with the two fiber-type particles (see Fig. 1b and 1c), a large number of CNT particles can be found around the NMC secondary particles compared to the number of VGCF particles. This is because fibers of VGCF particles are 5 times larger than that of CNT particles.

The cross-sectional view of the composite electrodes with the different CC is portrayed in Fig. 2(a-e). The pure NMC particles are directly embedded on the current collector due to compression. However, the active material and CC showed a fine distribution on the current collector, with the CC shielding the active material from direct contact with the current collector. The CC on the current collector ensures the continuous conduction of electrons between the current collector and the totality of the composite.

Table 2 shows the surface resistance of the pristine NMC electrode and the composite electrode with the various CC. The surface resistance of the composites decreases in the following order: NMC > NMC-SP > NMC-VGCF > NMC-KB > NMC-CNT. The incorporation of just 4 wt.% of the different CC significantly improved the inherent resistance of bare NMC. Comparing the fiber-like CC, the composite with CNT had less electrical resistance than VGCF. The microstructure and ordered graphitic nature of CNT is responsible for the excellent electronic conduction along its fibers compared to VGCF [10]. For the spherical particles, KB had less resistance compared to SP. This behavior can be associated with the particle sizes of the two CC. From Table 1, the particle size of SP and KB are 40 nm and 30 nm, respectively. It has been proven that electronic conductivity is significantly influenced by the size and shape of carbon additives in composites. The conductivity of various composites increases with decreasing particle size [26].

Table 2. Surface resistance, $A_{C/Al}$ and A_{mid} values of the composite electrodes with the different conductive carbons.

	Surface resistance (mW)	$A_{c/Al}$ (kNm^{-1})	A_{mid} (kNm^{-1})
NMC	3.21´106	0.721±0.0262	0.784±0.008
NMC-CNT	84	0.497±0.024	0.546±0.014
NMC-VGCF	115	0.467±0.008	0.331±0.002
NMC-KB	107	0.516±0.003	0.589±0.002
NMC-SP	122	0.357±0.002	0.408±0.005

The $A_{C/Al}$ and A_{mid} with regards to the different CC are shown in Table 2 and the corresponding data profile in Fig. 3. The electrodes with the different CC exhibited decreasing adhesion strength for the $A_{C/Al}$ and A_{mid} compared to the pure NMC electrode (see Table 2). Kim et al. has shown that higher adhesion strength recorded for the pure NMC composite electrode can be linked to the greater amount of heavy particles embedded directly on the current collector

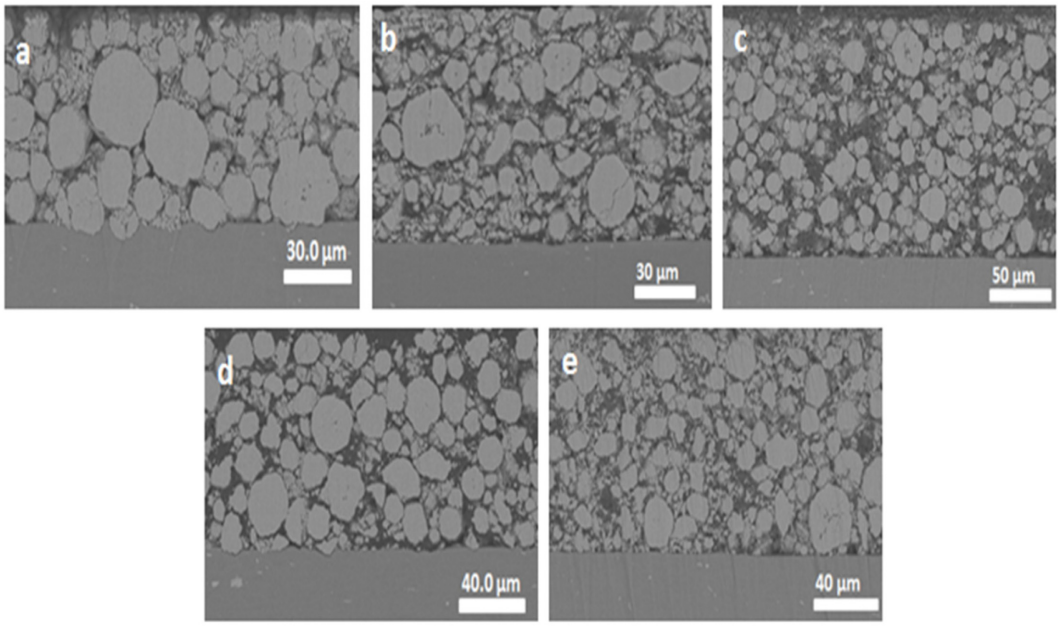

Fig. 2. Cross sectional images of the composites with the different conductive carbons (a) NMC, (b) NMC-CNT, (c) NMC-VGCF, (d) NMC-KB, and (e) NMC-SP.

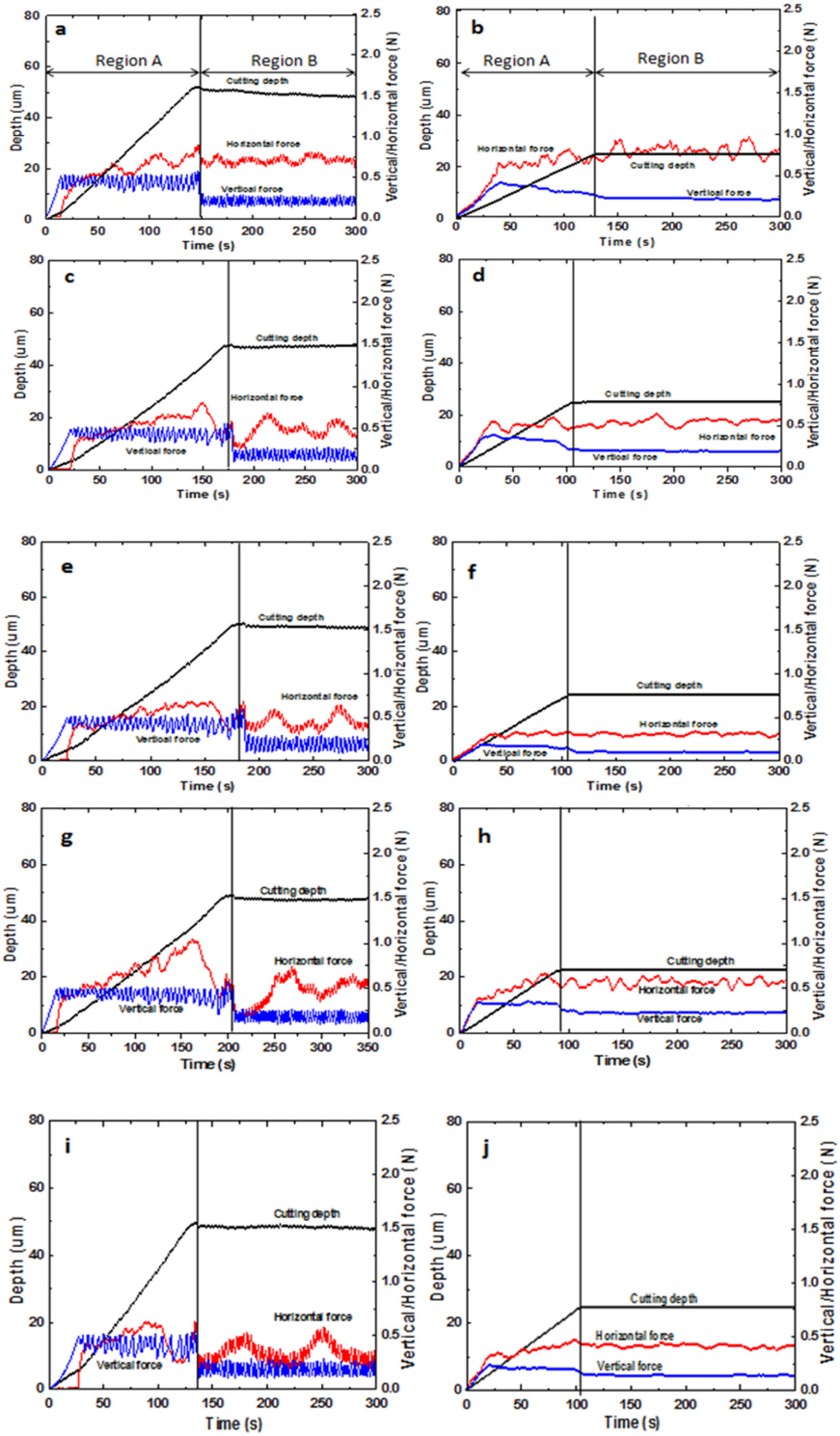

Fig. 3. SAICAS data profiles of $A_{C/Al}$ and A_{mid} for (a,b) NMC, (c,d) NMC –CNT, (e,f) NMC-VGCF, (g,h) NMC-KB, and (i,j)NMC-SP.

(see Fig. 2a) [23]. For the particle-like CC, the composite with SP showed the least $A_{C/Al}$ (0.357 kN m^{-1}) and A_{mid} (0.408 kN m^{-1}), and for the fiber-like carbon, VGCF displayed the least $A_{C/Al}$ (0.467 kN m^{-1}) and A_{mid} (0.331 kN m^{-1}). Examining the results, it can be concluded that the composites with KB and CNT had stronger $A_{C/Al}$ and A_{mid} due to their small particle size (see Table 1). The higher A_{mid} (which is recorded at the middle depth of the composite) recorded for the samples compared to the $A_{C/Al}$ can be connected to the additional physical interaction (electrostatic or Van der Waals forces associated with non-bonding interaction) between the active material and the CC [27]. These interactions have been found to be controlled by the particle size, aspect ratio, and morphology of the particles constituting the composite. Thus, the interaction and bonding between particles decrease with increased particle size and lower aspect ratio [28]. On the other hand, the reduced $A_{C/Al}$ may be due to the absence of these direct physical interactions of the composite film and the Al current collector. To be precise, the $A_{C/Al}$ (heterointerface) is solely due to the binding effect of PVdF. The lower A_{mid} recorded for the composite with VGCF could be associated with its fiber thickness. These thick fibers can hinder the binding property of PVdF as well as the interaction between the active material and the VGCF.

3.1 Cyclic voltammetry

The CV curves of the NMC with the various CC are shown in Fig. 4. All the samples showed a cathodic peak around 3.7 V and an anodic peak

Table 3. Redox peak potentials obtained from the CV data for the composite electrodes.

	Anodic peak (V)	Cathodic peak (V)	Peak separation (V)
NMC-CNT	3.871	3.723	0.148
NMC-VGCF	3.909	3.689	0.217
NMC-KB	3.870	3.711	0.159
NMC-SP	3.808	3.682	0.224

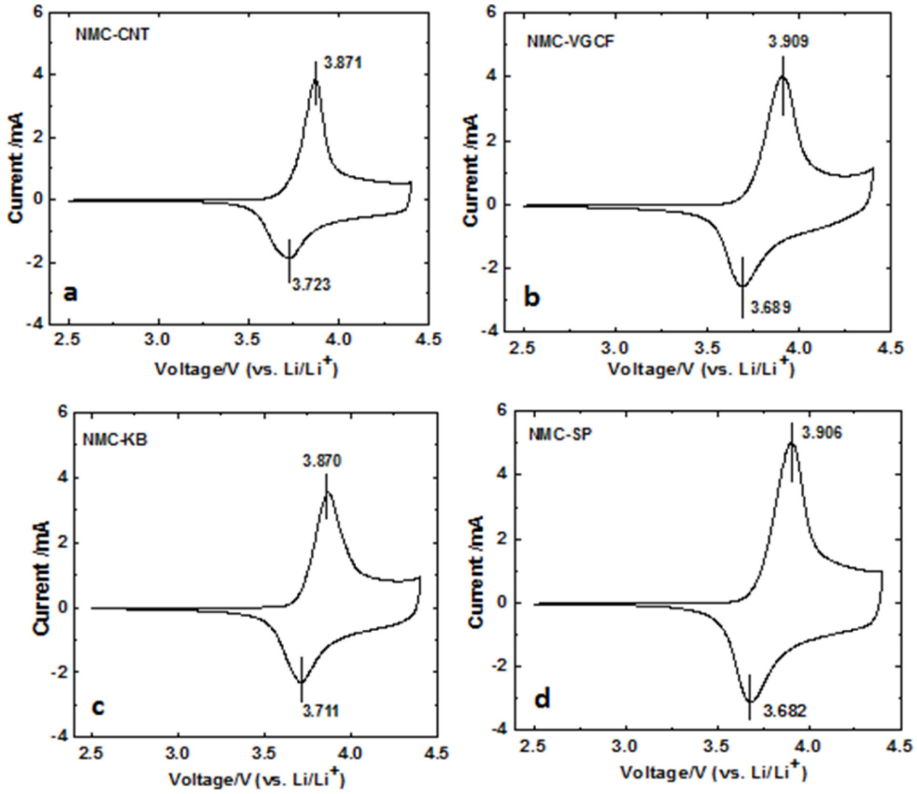

Fig. 4. CV curves of the NMC electrodes with the different conductive carbon from 2.5-4.4 V at a scan rate of 0.1 mV s^{-1}.

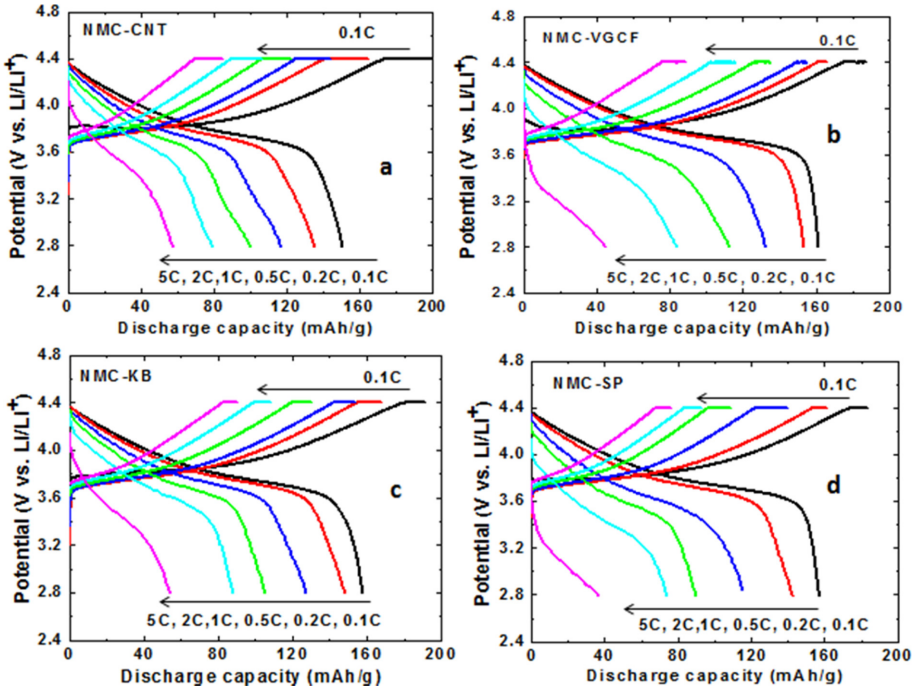

Fig. 5. Charge-discharge curves of NMC electrodes with the different conductive carbon from 2.5–4.4 V at different scan rates.

around 3.9 V, which resonates with other publications [29,30]. These peaks can be attributed to the redox reaction of Ni^{2+}/Ni^{4+}, during the insertion and deinsertion of lithium ions into the crystal structure of NMC. There is no peak corresponding to the reduction of Mn at 3.0 V; thus, it has an oxidation state of +4. According to Table 3, the oxidation-reduction peak separation ΔE ($E_{oxidation}$-$E_{reduction}$) increases in the order of NMC-CNT < NMC-KB < NMC-VGCF < NMC-SP, which means the composite with CNT and KB poses the least polarization; hence, the excellent rate capability observed in Fig. 5.

In addition, the charge-discharge capacities of the NMC with the different CC are depicted in Fig. 5. The curves of all the composites showed a similar charge-discharge plateau with a significant amount of capacity around 3.5-4.2 V, which corresponds to the redox transition of Ni^{2+}/Ni^{4+} in the structure of NMC. The fiber-like CC form a continuous conductive network connecting the different particles in the composite. This ensures the efficient passage of electrons through the composite. On the other hand, the particle-like CC lacks this continuous conductive network, and connects adjacent active material through direct point contact. This credible theory has been propagated by many researchers [8,10,12]. Nonetheless, results from $A_{C/Al}$ and A_{mid} indicate that the adhesion strength of the composite film on the current collector and the adhesion property between the particles of the composite are highly influenced by CC. The composite with VGCF and SP (Fig. 5a and 5b) demonstrated the highest polarization at a high C-rate with their discharge profiles shifting quickly toward lower potentials compared to the composites with CNT and KB (Fig. 5c and 5d). This phenomenon may be attributed to the reduced adhesion strength between the composite film and the current collector. Looking at Fig. 5 again, it can be seen that the composite with KB and CNT showed the best rate capability. There is strong evidence indicating that the high conductivity and the better adhesion played a synergistic role in providing these composite electrodes the best electrochemical performance. The cycle performance of the NMC electrodes with the different CC is depicted in Fig. 6a. The electrodes with CNT and KB, in particular, showed stable and higher capacity after 20 cycles.

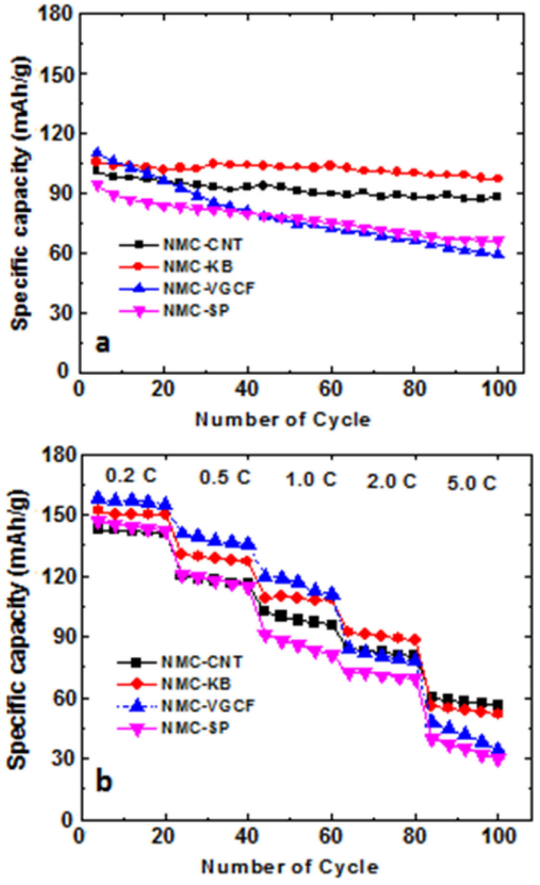

Fig. 6. a) Cycle performance and b) rate capability for the NMC electrodes with the different conductive carbons.

On the other hand, the electrodes with VGCF and SP showed decreasing capacity with an increasing number of cycles. This behavior can be closely related to the excellent adhesion exhibited by the composite consisting of CNT and KB due to their structure and particle size. Fig. 2b shows the rate capability of the NMC electrodes with the different CC. It can be observed that the electrodes with CNT and KB showed a noticeable increase in capacitance at lower C-rates compared to the electrodes with VGCF and SP. This can be attributed to the low resistance and better adhesion demonstrated by the composite with CNT and KB compared to the electrodes with VGCF and SP. This suggests that employing conductive particles with relatively smaller particle size is significantly improves the adhesion of composite electrodes. Multiple CC (two or more conductive particles) with reduced weight composition can be utilized to achieve better adhesion and thus enhance the electrochemical performance of composite electrodes. Finally, the surface treatment of current collectors may also be encouraged to reduce the interfacial resistance between the current collectors and the composite film.

4. Conclusions

In this work, we have successfully demonstrated the effect of fiber-like and particle-like CC on the adhesion strength of composite films on an Al current collector, and the strength of adhesion between the active material and the different CC. Electrodes with the different CC showed decreasing $A_{C/Al}$ and A_{mid} compared to the pure NMC electrode. The A_{mid} was stronger than the $A_{C/Al}$ for all the samples with the exception of the composite with VGCF. This behavior is attributed to the additional physical interactions between the active material and the different CC. The composite electrode with CNT showed better adhesion than VGCF as a result of their different fiber thickness. On the other hand, due to the smaller particle size of KB compared to SP, better adhesion was realized for the composite with KB. This outstanding $A_{C/Al}$ as well as the A_{mid} of the composite electrodes with KB and CNT facilitated rapid lithium ion and electron transfer. Consequently, lower electrode polarization, excellent cycle performance, and rate capability is achieved with the composite with CNT and KB compared to VGCF and SP. Thus, CC with smaller particle size is necessary for stronger $A_{C/Al}$ in order to achieve enhanced lithium ion battery performance.

References

[1] I. Doberdò, N. Löffler, N. Laszczynski, D. Cericola, N. Penazzi, S. Bodoardo, G.-T. Kim, S. Passerini, *J. Power Sources*, **2014**, *248*, 1000-1006.
[2] M.-H. Ryou, J. Kim, I. Lee, S. Kim, Y.K. Jeong, S. Hong, J.H. Ryu, T.-S. Kim, J.-K. Park, H. Lee, J.W. Choi, *Adv. Mater*, **2012**, *25(11)*, 1571-1576.
[3] J. Chong, S. Xun, H. Zheng, X. Song, G. Liu, P. Ridgway, J.Q. Wang, V.S. Battaglia, *J. Power Sources*, **2011**, *196(18)*, 7707-7714.
[4] S.-L. Chou, J.-Z. Wang, H.-K. Liu, S.-X. Dou, *J. Phys. Chem. C*, **2011**, *115(32)*, 16220-16227.
[5] Z.-J. Han, N. Yabuuchi, S. Hashimoto, T. Sasaki, S.

Komaba, *ECS Electrochem. Lett.*, **2013**, *2(2)*, A17-A20.
[6] B. Tran, I.O. Oladeji, Z. Wang, J. Calderon, G. Chai, D. Atherton, L. Zhai, *J. Electrochem. Soc.*, **2012**, *159(12)*, A1928-A1933.
[7] G. Liu, H. Zheng, X. Song, V.S. Battaglia, *J. Electrochem. Soc.*, **2012**, *159(3)*, A214-A221.
[8] S. Ahn, Y. Kim, K.J. Kim, T.H. Kim, H. Lee, M.H. Kim, *J. Power Sources*, **1999**, *81-82*, 896-901.
[9] X. Shen, C. Wang, J. Dong, *US20040121236 A1*, **2004**.
[10] W. Guoping, Z. Qingtang, Y. Zuolong, Q. MeiZheng, *Solid State Ionics*, **2008**, *179(7-8)*, 263-268.
[11] J. Kim, B. Kim, J.-G. Lee, J. Cho, B. Park, *J. Power Sources*, **2005**, *139(1-2)*, 289-294.
[12] M. Hibino, H. Kawaoka, H. Zhou, I. Honma, *J. Power Sources*, **2003**, *124(1)*, 143-147.
[13] A. Sakuda, N. Nakamoto, H. Kitaura, A. Hayashi, K. Tadanaga, M. Tatsumisago, *J. Mater. Chem.*, **2012**, *22*, 15247-15254.
[14] Hyperion Catalysis International, Nanotube Technology, http://hyperioncatalysis.com/technology2.htm (Accessed on: Jan 4, 2018).
[15] C. Lampe-Onnerud, J. Shi, P. Onnerud, R. Chamberlain, B. Barnett, *J. Power Sources*, **2001**, *97-98*, 133-136.
[16] S.K. Vanimisetti, N. Ramakrishnan, *Proc. Inst. Mech. Eng. C*, **2012**, *226(9)*, 2192-2213.
[17] K.Y. Song, G.S. Jang, J. Tao, J.H. Lee, S.K. Joo, *J. Electrochem. Soc.*, **2016**, *163(14)*, A2981-A2987.
[18] H. Li, H. Zhou, *Chem. Commun.*, **2012**, *48*, 1201-1217.
[19] S. Nakanashi, T. Suzuki, Q. Cui, J. Akikusa, K. Nakamura, *Trans. Nonferrous Met. Soc. China*, **2014**, *24*, 2314-2319.
[20] Y.K. Jeong, T.-W. Kwon, I. Lee, T.-S. Kim, A. Coskun, J.W. Choi, *Energy Enviro. Sci.* **2015**, *8*, 1224-1230.
[21] Y.K. Jeong, T.-W. Kwon, I. Lee, T.-S. Kim, A. Coskun, J.W. Choi, *Nano Lett.*, **2014**, *14(2)*, 864-870.
[22] W. Haselrieder, B. Westphal, H. Bockholt, A. Diener, S. Höft, A. Kwade, *Int. J. Adhes. Adhes.*, **2015**, *60*, 1-8.
[23] Bongki, Son, M.-H. Ryou, J. Choi, T. Lee, H.K. Yu, J.H. Kim, Y.M. Lee, *ACS Appl. Mater. Interfaces*, **2014**, *6(1)*, 526-531.
[24] J. Choi, K. Kim, J. Jeong, K.Y. Cho, M.-H. Ryou, Y.M. Lee, *ACS Appl. Mater. Interfaces*, **2015**, *7(27)*, 14851-14858.
[25] K. Kim, S. Byun, I. Cho, M.-H. Ryou, Y.M. Lee, *ACS Appl. Mater. Interfaces*, **2016**, *8(36)*, 23688-23695.
[26] C.A. Frysz, X. Shui, D.D.L. Chung, *J. Power Sources*, **1996**, *58(1)*, 41-54.
[27] M. Wong, M. Paramsothy, X.J. Xu, Y. Ren, S. Li, K. Liao, *Polym.*, **2003**, *44(25)*, 7757-7764.
[28] S.-Y. Fu, X.-Q. Feng, B. Lauke, Y.-W. Mai, *Composites Part B*, **2008**, *39(6)*, 933-961.
[29] J. Xu, F. Lin, M.M. Doeff, W. Tong, *J. Mater. Chem. A*, **2017**, *5*, 874-901.
[30] M. Ma, N.A. Chernova, B.H. Toby, P.Y. Zavalij, M.S. Whittingham, *J. Power Sources*, **2007**, *165(2)*, 517-534.